Role of pore morphology in positronium diffusion in mesoporous silica thin films and in positronium emission from the surfaces

Chunqing He[*] and Shaojie Wang

Key Lab of Nuclear Solid Physics Hubei Province, School of Physics and Technology, Wuhan University, Wuhan 430072, China

Yoshinori Kobayashi,[†] Toshiyuki Ohdaira, and Ryoichi Suzuki

National Institute of Advanced Industrial Science and Technology (AIST), Tsukuba, Ibaraki 305-8565 and 305-8568, Japan

Diffusion of *ortho*-positronium (*o*-Ps) in mesoporous silica films with different pore morphologies and its emission from the surfaces were studied using the Ps time-of-flight method and positron annihilation γ-ray energy spectroscopy. Probabilities of *o*-Ps formation are almost the same in the studied films, however, the emission intensity of *o*-Ps from the film with much larger cagelike pores is significantly less than that from the film with much smaller tubelike pores, where Ps diffusion between cages is feasible by tunneling. A simple strategy is suggested to use mesoporous silica film for the generation of dense enough Ps for many-positronium experiments.

Positronium (Ps), the metastable electron-positron bound state, has been an object of intensive investigations in diverse fields including material science and fundamental physics. Ps has been used as a unique probe of defects and nanopores in semiconductors and insulators for modern microelectronics.[1] More recently, considerable attention has been directed toward high precision spectroscopy of excited Ps,[2] Ps Bose-Einstein condensation (Ps-BEC), and Ps annihilation γ-ray laser,[3,4] in addition to the use of Ps for the production of antihydrogen[5,6] and antimatter gravity measurements.[7,8] Using a Surko-trap-based[9] intense positron beam, Cassidy and Mills *et al.* succeeded in observing Ps-Ps interaction/spin-polarized Ps gas and Ps$_2$ molecule formation in mesoporous silica films,[10–12] which is definitely a milestone toward Ps-BEC. For the ultimate achievement of Ps-BEC, however, creation of dense enough Ps confined in a small space is still a challenge.

After being injected in porous silica films, a fraction of the positrons can capture electrons from surrounding atoms and form Ps. The Ps easily gets trapped in pores and loses its kinetic energy by colliding with the pore walls. Cooled-down Ps could diffuse over a long distance inside the pores, reach the surface, and be emitted out to vacuum, if the pores are open to the outside. Detecting annihilation γ rays of Ps from mesoporous targets with such techniques as Ps time-of-flight (Ps-TOF) and annihilation γ-ray spectroscopy, one can obtain information on its cooling process.[2,13,14] It takes a short period of a few hundred picoseconds for Ps to cool down from ∼1 eV to several hundred meV in nanopores, however, for further cooling below the latter energy it takes much longer.[13–15] Nevertheless, Ps is seldom emitted from nanopores/nanochannels with thermal energy because of its quantum confinement in them.[2,16,17]

Despite the recent discovery of efficient Ps emission from laser-irradiated p-Si(110) via a positronic excitonlike state by Cassidy *et al.*,[18,19] mesoporous silica film is still believed to be a proper target for generating high density Ps. This is because a wide variety of nanostructures can be introduced into the mesoporous silica film by a sol-gel process using templates. Nagashima *et al.* studied Ps in gas-filled silica

aerogel and showed that a classical model can well explain the thermalization of Ps in it.[13] However, Ps formation, diffusion, and cooling in mesoporous silica films strongly depend on the pore characteristics, such as porosity, pore interconnectivity, pore surface,[14] and pore shapes. In this letter, we study the behavior of Ps in mesoporous silica films using Ps-TOF[14] and positron annihilation γ-ray energy spectroscopy.[20] The Ps 3γ annihilation data are compared with Monte Carlo simulation of Ps diffusion by random walks. The nanopore morphology has a significant impact on Ps cooling and diffusion in mesoporous silica films, so there is a hope to generate Ps in higher density by optimizing the nanoporous structure of the mesoporous silica film.

Mesostructural silica films were synthesized via a sol-gel process as described previously[21,22] using triblock copolymers F38 and F127 (BASF surfactants) with different molecular weights as the structure-directing agents and tetraethoxysilane (TEOS) as the network backbone precursor, respectively. The coating solutions were prepared by the addition of ethanol solutions of triblock copolymers to silica sols. The precursor sols were dip-coated on polished Si(100) wafers and calcined at an elevated temperature to decompose the templates. Mesoporous silica films thus prepared with F38 and F127 are denoted as samples A and B, respectively. Thicknesses of films A and B are determined to be 246 and 294 nm, respectively, by spectroscopic ellipsometry. Positron annihilation lifetime spectra were measured at an incident positron energy of 2 keV for the films capped with 20-nm-thick nonporous SiO$_2$, using positron annihilation lifetime spectroscopy (PALS) based on the intense pulsed positron beam at the National Institute of Advanced Industrial Science and Technology (AIST).[23,24] The lifetime spectra were resolved into a sum of exponential terms and the longest-lived *o*-Ps components with lifetimes of 46.5 ns for A and 68.3 ns for B were attributed to the annihilation of *o*-Ps in the mesopores. The total intensities of *o*-Ps in the mesopores were ∼25% for both the samples.[20] The much longer *o*-Ps lifetime in sample B indicates that its pore size is far larger than A. Spectroscopic ellipsometry combined with heptane gas adsorption [ellipsometric porosimetry (EP)] and
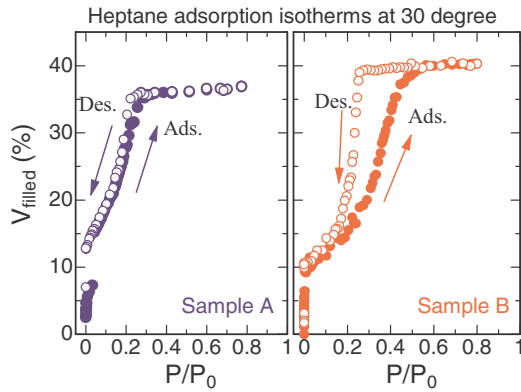
FIG. 1. (Color online) Heptane adsorption isotherms at 30 °C for films A and B obtained by ellipsometric porosimetry (EP).

transmission electron microscopy (TEM) were used to explore the pore morphology of the two films.

Figure 1 depicts the heptane vapor adsorption isotherms measured at 30°C. From the change of film refractive index at 30°C the fractional volumes filled by condensed gas vapor were obtained as a function of the specific gas pressure (i.e., the ratio of the gas pressure to its saturation vapor pressure). There is little difference in the adsorption and desorption branches for sample A, however, a significant adsorption-desorption hysteresis loop is observed for B. Thus the pores in B are more heterogeneous in size and likely consist of cages interconnected via channels (cagelike). On the other hand, pores in A are more uniform in diameter and probably tubular or channel-like. Total mesoporosities of A and B are estimated to be 37% and 40%, respectively. The large amounts of heptane adsorption indicate that mesopores in both A and B are well interconnected, and the "cages" in the pores of B are not isolated. The different pore morphologies of the two films were further confirmed by TEM observation (Fig. 2). As indicated by the arrows, wormlike tubular pores and *isolated* spherical cages are visible in the images of samples A and B, respectively. Taking the different pore morphologies into consideration, the pore sizes of the two films were calculated from PALS data. Assuming rectangular pores, the pore size of A was calculated
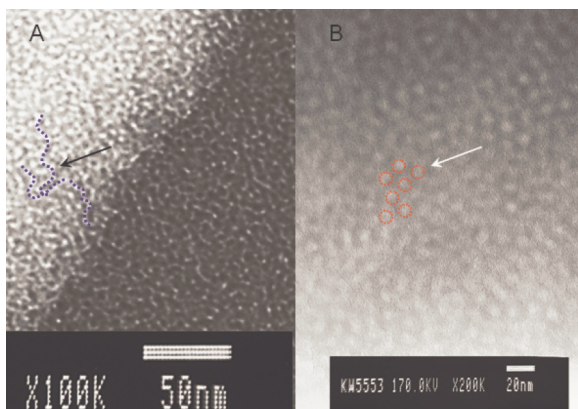
FIG. 2. (Color online) Pores in films A and B observed by transmission electron microscopy (TEM). Arrows indicate wormlike tubular pores and *isolated* spherical cages in films A and B, respectively.
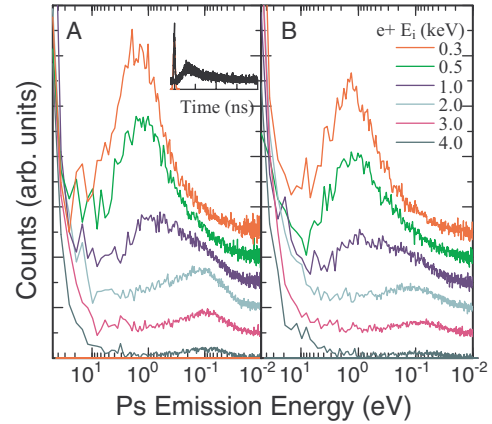
FIG. 3. (Color online) Energy distributions of Ps emitted from films A and B, converted from Ps time-of-flight spectra. The energy distribution curves of Ps (up to down) correspond to the incident positron energies of 0.3, 0.5, 1.0, 2.0, 3.0, and 4.0 keV, respectively. The inset in sample A shows a typical raw Ps-TOF spectrum.

3.0 nm, whereas the cage size of B was calculated 5.6 nm assuming cubic pores based on the rectangular Tao-Eldrup model.[25] Thus, the pores in A are rather uniform channels of 3 nm in diameter, but those in sample B are "cages" of 5.6 nm, connected by channels with smaller diameter ∼2.5 nm according to the desorption branch of the isotherm.

Figure 3 displays Ps emission energy spectra at different incident positron energies obtained from Ps-TOF experiments on the two samples. Annihilation γ rays due to the intrinsic decay of o-Ps in flight over a fixed distance of 1.5 cm were detected by two scintillators each placed behind a lead slit with 5-mm width. Ps-TOF spectra were recorded using a time-to-amplitude converter started by the detected γ rays and stopped by the timing signals of the pulsing system. More details of TOF measurements of positrons and Ps can be found elsewhere.[14,26–28] The inset in Fig. 3 (film A) shows a typical Ps-TOF spectrum, where the prompt annihilation peak is ∼3-ns [full width at half maximum (FWHM)] wide. As-recorded Ps-TOF spectra were corrected by multiplying $(1/t)\exp(t/142 \text{ ns})$ after subtraction of random background and subsequently normalized. The time scale was converted to the energy scale taking account of the relationship between the flight time T_f and Ps kinetic energy $E_\perp$ [i.e., $E_\perp = m_e(l/T_f)^2$], where m_e is the positron rest mass and l is the o-Ps flight distance. As displayed in Fig. 3, when the incident positron energy is lower than ∼1.0 keV, the peak emission energies of Ps from the two films are between 1.0 and 2.0 eV. With increasing implantation energy, the peak Ps emission energies gradually shift to lower energies and reach ∼0.1 eV for the two films. No significant difference in Ps emission energy was observed between the two films, but Ps emission intensity at each incident energy was much higher for A than B.

Ps-TOF spectra recorded at positron implantation energies less than 1.0 keV show appreciable asymmetry at relatively high Ps emission energies. Similar asymmetry was observed for Ps emission from porous silicon containing straight channels with decorated inner SiO_2 walls by Mariazzi *et al.*,[15] but at higher incident energies up to 7 keV. The channels in porous silicon are different from the pores in our films; they
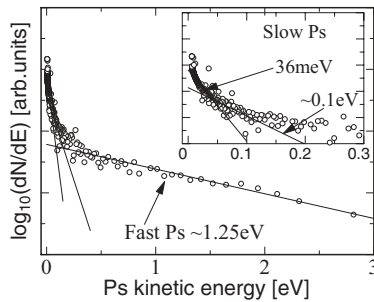
FIG. 4. Ps emission energy spectra at an implantation energy of 3.0 keV for film A in a semilog scale obtained by multiplying t^3 for the corresponding Ps-TOF spectrum. Inset shows the enlarged spectrum at low Ps kinetic energies. Fittings were done in the three regions, from ~10 to ~50 meV, from ~45 to ~120 meV, and from ~0.25 to ~3.0 eV for thermal Ps, cooled Ps, and fast Ps, respectively.

are 5 nm in size and aligned perpendicularly to the sample surface. These authors plotted the Ps-TOF spectra multiplied by t^3 in a semilog scale and demonstrated emission of cooled Ps with thermal energy at cryogenic temperature. We plotted our Ps-TOF spectra in the same way as Mariazzi *et al.*[15] Such a plot for sample A at 3 keV is presented in Fig. 4, which reveals exponential distributions of Ps emission energies. The high energy part of the spectrum can be well fitted with a single Ps emission energy of 1.25 eV, which obviously originates from direct emission of uncooled Ps from the pores and the film surface.[28] The low energy part of the spectrum, corresponding to cooled Ps emission, shows a wide distribution ranging from 36 meV to several hundred meV. The distribution is peaked at around 86 meV. Taking account of the Ps quantum confinement effect, the lowest attainable energy of Ps emission from a spherical nanopore with radius a (diameter d) should be[2] $E_0 = \pi^2 \hbar^2 / 2 m_{Ps} a^2 \sim 753$ meV$(1 \text{ nm}/d)^2$. This relationship provides 84 meV as the ground-state energy for Ps in a pore of 3 nm, which agrees with the observed emission energy ~86 meV for Ps from sample A. For sample B with the cages of 5.6 nm in diameter, the zero-point energy of confined Ps should be 30 meV, which seems far from the experimental value (i.e., ~120 meV), obtained by fitting of Ps energy spectrum at an incident energy of 3 keV. Nevertheless, the value becomes quite reasonable if we consider that Ps is emitted from the channels of ~2.5 nm connecting the cages as mentioned above. Careful analysis of the Ps emission energy spectrum in the inset of Fig. 4 shows a small fraction of Ps with energy ~36 meV, which could be thermally desorbed Ps from the trapped state on the film surface.[15,29]

Thus, Ps emitted from the pores of porous silica film mainly is of two types: One is the fast, uncooled Ps emitted directly from the film after rare collisions inside the pores. The other is the slow Ps emitted after numerous collisions inside the pores. The peak energy $E_\perp \sim 1$ eV of the former type of Ps hardly changes with increasing incident energy up to 1.0 keV (Fig. 4); only does the emission intensity of such Ps decrease with incident energy. When positrons are injected deeply inside the film, the probability of fast Ps emission from the film surface is much reduced. Instead, slow Ps emission becomes dominant. More Ps emission may be expected for films with higher open porosity, but this is not the case for our film B. This
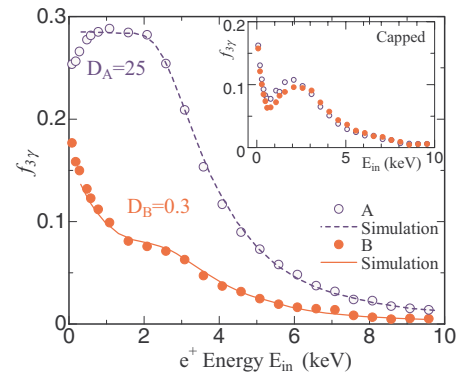
FIG. 5. (Color online) Positron 3γ-annihilation fraction $f_{3\gamma}$ as a function of positron implantation energy in the two films. Inset shows the data for the films capped with a 20-nm nonporous SiO_2 layer on their surfaces. Lines were obtained by Monte Carlo simulations via a random walk method, by adjusting the D parameter that is a step length, relevant to the Ps diffusion coefficient, of the random walk diffusion model.

film has essentially the same Ps formation probability, slightly higher porosity, and much larger pores than A. However, the Ps emission intensity at any incident energy is considerably less in this film than A. The remarkable difference in Ps emission between A and B has to do with the different pore morphologies of the two films. To elucidate the role of pore morphology in Ps diffusion in mesoporous silica, positron annihilation γ-ray energy spectra were measured as a function of positron incident energy from 100 eV up to 30 keV for the two samples. 3γ annihilation fractions $f_{3\gamma}$ were calculated as described in Ref. 30 using silicon (no Ps formation in bulk) and aerogel (~98% Ps formation) as reference samples.

Figure 5 displays the absolute positron 3γ annihilation fraction $f_{3\gamma}$ in the two samples as a function of positron implantation energy. The inset shows $f_{3\gamma}$ for the two films with a 20-nm-thick nonporous SiO_2 capping layer. There is little difference in $f_{3\gamma}$ between A and B. For uncapped films, a dramatic difference in $f_{3\gamma}$ can be seen between A and B because of the difference in Ps emission. In uncapped film A, $f_{3\gamma}$ increases slightly at low incident energies due to the increased Ps formation.[31] It then attains a plateau of ~28% at implantation energies from ~0.8 to ~2.5 keV, where most positrons are stopped in the films. Considering $f_{3\gamma}$ in uncapped film A and the Ps intensity of 27.7% (from PALS) in the capped one, it is rational to state that Ps diffuses easily over a long distance in the pores and can be emitted out from the film surface. With further increase in positron incident energy more positrons are stopped in the silicon substrate and $f_{3\gamma}$ decreases. However, for uncapped film B $f_{3\gamma}$ decreases gradually from near surface and reaches a plateau of only ~8%, when the positrons are stopped in the film. It then decreases with increasing incident energy due to the positron implantation into the substrate. The capping of film B does not influence Ps emission so much as film A, indicating Ps diffusion is rather difficult in the former film in spite of its high open porosity and the large size of the cagelike pores.

A rough estimation[2] based on the measured density (~1.24 g/cm^3) and pore size (~5.6 nm) of film B shows that the distance between the neighboring cages is ~17.5 nm,

which agrees well with TEM observation. This means that the connecting channel of $\sim$2.5 nm in diameter is $\sim$11.9-nm long. Ps de Broglie wavelength λ_{Ps} at kinetic energy E_{Ps} is obtained from $\lambda_{Ps} = h(2m_{Ps}E_{Ps})^{-1/2} \sim 0.9$ nm$(1 \text{ eV}/E_{Ps})^{1/2}$.[2] Given that cooled Ps with $\sim$120 meV is trapped in the cagelike pore of film B, then its wavelength is $\sim$2.6 nm. This is much shorter than the channel length, therefore, Ps diffusion by tunneling is unlikely. On the other hand, for thermalized Ps in such a cage, the wavelength is $\sim$6.3 nm comparable to half the connecting channel length. Meanwhile, the ground-state energy of Ps ($\sim$120 meV) in the channel is much higher than in the cage, so that cooled Ps has low probability to tunnel from one cage to another. In sample A, where the pores are well-connected channels, cooled Ps with a wavelength of $\sim$3 nm likely diffuses over a long distance through tunneling up to a few microns before it is emitted out from film surface or annihilates in the pores.

For deeper understanding of the Ps diffusion in mesoporous films and its emission from the surface, Monte Carlo simulation was carried out. Although the diffusion process of cooled Ps can be dominated by Ps tunneling, where the Ps atom hops from a pore to another with a fixed path length, one is still able to use the diffusion model to describe the process by using a modified diffusion coefficient.[32] Thus, we used a one-dimensional random walk model to simulate Ps diffusion in porous films as previously reported.[33] The film density and thickness were fixed to the measured values (i.e., 1.29 g/cm^3 and 246 nm for sample A, and 1.24 g/cm^3 and 294 nm for sample B, respectively). In the simulation, the step of walk D relevant to the Ps diffusion coefficient was varied from 0.01 to 30. By comparing the simulated $f_{3\gamma}$ curves with the experimental data, good fittings were obtained with $D_A = 25$ and $D_B = 0.3$ for samples A and B, respectively. This result clearly shows that indeed the Ps diffusion coefficient is much higher in sample A, whose tubular pores are smaller and consist of interconnected spherical cages. For Ps in a mesoporous film with tubular pores, the one-dimensional diffusion coefficient D_{Ps} can be approximated to be $\bar{v} \times l$, where $\bar{v}$ and l are the Ps mean velocity and the mean free path/pore diameter. According to Ps-TOF results, the mean Ps velocity $\bar{v}$ in sample A with 3-nm tubular pores is about 10^7cm/s, which gives $D_{Ps} \sim 3$ cm^2/s. One may expect that Ps has a higher diffusion coefficient in film B with almost twice larger cagelike pores. However, the comparison of the obtained D parameters for the two films reveals that Ps diffusion coefficient D_{Ps} for film B is $\sim$0.04 cm^2/s, approximately two orders of magnitude lower than that of film A. This means that the diffusion of the Ps atom between the cages in film B is difficult because of its strong confinement in the cages. The high diffusion coefficient of Ps in tubular nanopores could have resulted in a lower Ps local density in high density Ps experiments using porous silica films by Cassidy *et al.*,[10] in which the Ps surface state and Ps spin exchange quenching were not observed. Furthermore, the low
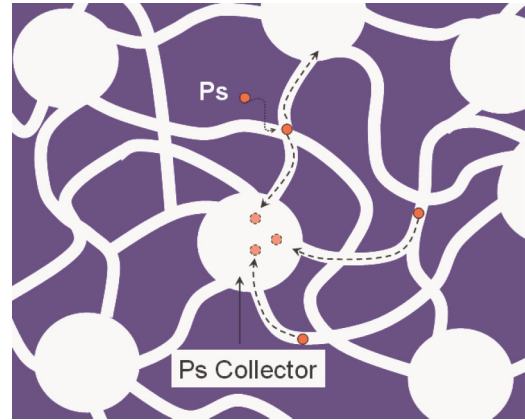
FIG. 6. (Color online) Schematic image of a Ps accumulator using mesoporous silica film.

diffusion rate of Ps confined in the cages may explain the recent observation of the enhanced Ps-Ps interactions in some porous silica films by the same authors.[34]

In summary, we have observed that Ps has a much higher diffusion rate in the smaller tubular pores than the pores consisting of connected larger cages, where Ps is preferentially localized in the cages during diffusion. As mentioned by Cassidy *et al.*,[11] cooled Ps can be accumulated in larger pores or nanocavities. Our present results clearly show that the mesoporous film with nanopores of desired morphology can be used as a medium to collect dense enough Ps. Mesoporous silica film consisting of cagelike pores/nanocavities in $\sim$20-nm size that are well connected to a number of long tubelike pores of smaller size ($\sim$3 nm, for instance) can be used for this purpose (Fig. 6). Ps formed in the film may migrate from micropores to tubular pores and get trapped therein. The trapped Ps diffuses inside the tubes and finally is *collected* and *accumulated* in large cages/cavities as *cooled* Ps. Using the currently available positron beam[2] with a central area density up to 10^{11}e$^+$/cm^2 and pulse width 1 ns, and on assumption of 40% Ps formation and a cage separation of 200 nm in such a mesoporous silica film with several hundred nanometers in thickness, it seems feasible to attain an *effective* Ps density up to $\sim$10^{18}/cm^3 in the large cages. Such a Ps density is suitable for the studies of many Ps physics.

---

*hecq@whu.edu.cn

†y-kobayashi@aist.go.jp

[1]D. W. Gidley, H. G. Peng, and R. S. Vallery, Annu. Rev. Mater. Res. **36**, 49 (2006).

[2]D. B. Cassidy, P. Crivelli, T. H. Hisakado, L. Liszkay, V. E. Meligne, P. Perez, H. W. K. Tom, and A. P. Mills, Jr., Phys. Rev. A **81**, 012715 (2010).

[3]P. M. Platzman and A. P. Mills, Jr., Phys. Rev. B **49**, 454 (1994).

[4] A. P. Mills, Jr., Radiat. Phys. Chem. **76**, 76 (2007).

[5] M. Charlton, Phys. Lett. A **143**, 143 (1990).

[6] M. Amoretti *et al.*, Nature (London) **419**, 456 (2002).

[7] A. P. Mills, Jr. and M. Leventhal, Nucl. Instrum. Methods B **192**, 102 (2002).

[8] Michael Doser (the Aegis collaboration), J. Phys.: Conf. Ser. **199**, 012009 (2010).

[9] C. M. Surko and R. G. Greaves, Phys. Plasmas **11**, 2333 (2004).

[10] D. B. Cassidy and A. P. Mills, Jr., Phys. Rev. Lett. **100**, 013401 (2008).

[11] D. B. Cassidy, V. E. Meligne, and A. P. Mills, Jr., Phys. Rev. Lett. **104**, 173401 (2010).

[12] D. B. Cassidy and A. P. Mills, Jr., Nature (London) **449**, 195 (2007).

[13] Y. Nagashima, M. Kakimoto, T. Hyodo, K. Fujiwara, A. Ichimura, T. Chang, J. Deng, T. Akahane, T. Chiba, K. Suzuki, B. T. A. McKee, and A. T. Stewart, Phys. Rev. A **52**, 258 (1995).

[14] C. He, T. Ohdaira, N. Oshima, M. Muramatsu, A. Kinomura, R. Suzuki, T. Oka, and Y. Kobayashi, Phys. Rev. B **75**, 195404 (2007).

[15] S. Mariazzi, P. Bettotti, and R. S. Brusa, Phys. Rev. Lett. **104**, 243401 (2010).

[16] S. Mariazzi, A. Salemi, and R. S. Brusa, Phys. Rev. B **78**, 085428 (2008).

[17] P. Crivelli, U. Gendotti, A. Rubbia, L. Liszkay, P. Perez, and C. Corbel, Phys. Rev. A **81**, 052703 (2010).

[18] D. B. Cassidy, T. H. Hisakado, H. W. K. Tom, and A. P. Mills, Jr., Phys. Rev. Lett. **106**, 133401 (2011).

[19] D. B. Cassidy, T. H. Hisakado, H. W. K. Tom, and A. P. Mills, Jr., Phys. Rev. Lett. **107**, 033401 (2011).

[20] C. He, T. Oka, Y. Kobayashi, N. Oshima, T. Ohdaira, A. Kinomura, and R. Suzuki, Appl. Surf. Sci. **255**, 183 (2008).

[21] D. Zhao, J. Feng, Q. Huo, N. Melosh, G. H. Fredrickson, B. F. Chmelka, and G. D. Stucky, Science **279**, 548 (1998).

[22] C. He, M. Muramatsu, T. Ohdaira, N. Oshima, A. Kinomura, R. Suzuki, and Y. Kobayashi, Radiat. Phys. Chem. **76**, 204 (2007).

[23] R. Suzuki, T. Mikado, H. Ohgaki, M. Chiwaki, T. Yamazaki, and Y. Kobayashi, Phys. Rev. B **49**, 17484 (1994).

[24] T. Yamazaki, R. Suzuki, T. Ohdaira, T. Mikado, and Y. Kobayashi, Radiat. Phys. Chem. **49**, 651 (1997).

[25] D. W. Gidley, W. E. Frieze, T. L. Dull, A. F. Yee, E. T. Ryan, and H. M. Ho, Phys. Rev. B **60**, R5157 (1999).

[26] A. P. Mills, L. Pfeiffer, and P. M. Platzman, Phys. Rev. Lett. **51**, 1085 (1983).

[27] A. P. Mills, E. D. Shaw, R. J. Chichester, and D. M. Zuckerman, Phys. Rev. B **40**, 2045 (1989).

[28] Y. Nagashima, Y. Morinaka, T. Kurihara, Y. Nagai, T. Hyodo, T. Shidara, and K. Nakahara, Phys. Rev. B **58**, 12676 (1998).

[29] A. P. Mills, E. D. Shaw, M. Leventhal, R. J. Chichester, and D. M. Zuckerman, Phys. Rev. B **44**, 5791 (1991).

[30] Y. Kobayashi, W. Zheng, T. B. Chang, H. Hirata, R. Suzuki, T. Ohdaira, and K. Ito, J. Appl. Phys. **91**, 1740 (2002).

[31] M. P. Petkov, M. H. Weber, K. G. Lynn, and K. P. Rodbell, Appl. Phys. Lett. **79**, 3884 (2001).

[32] D. B. Cassidy, T. H. Hisakado, V. E. Meligne, H. W. K. Tom, and A. P. Mills, Jr., Phys. Rev. A **82**, 052511 (2010).

[33] R. Suzuki, T. Ohdaira, Y. Kobayashi, K. Ito, R. S. Yu, Y. Shioya, H. Ichikawa, H. Hosomi, K. Ishikiriyama, H. Shirataki, S. Mastuno, and J. Xu, Mater. Sci. Forum **445–446**, 224 (2004).

[34] D. B. Cassidy and A. P. Mills, Jr., Phys. Rev. Lett. **107**, 213401 (2011).